

JGR Space Physics

RESEARCH ARTICLE

10.1029/2018JA026103

Key Points:

- A deep ingressions of the MSTID to a very low geomagnetic latitude is noted during the descending phase of the 24th solar cycle
- Quasiperiodic southward moving waves (QPSMW) and a small-scale southward moving wave signature are also observed in addition with the MSTID
- The dissipation of all these features is possibly due to existence of the midnight pressure bulge (MPB)

Supporting Information:

- Supporting Information S1
- Data Set S1
- Data Set S2
- Data Set S3
- Data Set S4

Correspondence to:

M. Sivakandan,
skandanm89@gmail.com;
sivakandan@prl.res.in

Citation:

Sivakandan, M., Chakrabarty, D., Ramkumar, T. K., Guharay, A., Taori, A., & Parihar, N. (2019). Evidence for deep ingressions of the midlatitude MSTID into as low as $\sim 3.5^\circ$ magnetic latitude. *Journal of Geophysical Research: Space Physics*, 124, 749–764. <https://doi.org/10.1029/2018JA026103>

Received 15 SEP 2018


Accepted 19 NOV 2018

Accepted article online 8 JAN 2019

Published online 30 JAN 2019

©2019. American Geophysical Union.
All Rights Reserved.

Evidence for Deep Ingression of the Midlatitude MSTID Into As Low as $\sim 3.5^\circ$ Magnetic Latitude

M. Sivakandan¹ , D. Chakrabarty¹ , T. K. Ramkumar² , A. Guharay¹, A. Taori³ , and N. Parihar⁴ 

¹Physical Research Laboratory, Ahmedabad, India, ²National Atmospheric Research Laboratory, Gadanki, India, ³Regional Remote Sensing Centre- Central, Nagpur, India, ⁴Equatorial Geophysical Research Laboratory, Indian Institute of Geomagnetism, Tirunelveli, India

An observational evidence of medium-scale traveling ionospheric disturbances (MSTIDs) reaching to magnetic latitude as low as $\sim 3.5^\circ$ over the Indian sector is provided for the first time based on OI 630-nm airglow imaging observation from a low-latitude station, Gadanki (13.5°N , 79.2°E ; 6.6° magnetic latitude), on 12 January 2016. The horizontal wavelength, horizontal phase velocity, and period of the MSTID are found to be 160 ± 6 km, 138 ± 14 m/s, and 19.5 ± 3 min, respectively. These phase fronts are observed to move toward southwest with a propagation angle of $\sim 235^\circ \pm 1^\circ$ with respect to north. In addition to the MSTID, a strong quasiperiodic southward moving wave (QPSMW) from the evening to midnight interval and a small-scale southward moving wave structure with wavelength and periodicity different from the QPSMW are also detected on the same night. Horizontal wavelength, horizontal phase velocity, and period of the QPSMW are estimated to be 367 ± 14 km, 131 ± 18 m/s, and 46.7 ± 13 min, respectively, and those of the small-scale southward moving wave are found to be 157 ± 4 km, 121 ± 17.8 m/s, and 21.7 ± 3.4 min, respectively. Global Positioning System-total electron content maps suggest that the weak and asymmetric equatorial ionization anomaly helped deep ingression of the MSTID on this night. The descent of the F layer seems to have caused the dissipation of the MSTID and QPSMW closer to the dip equator on this night. Therefore, the present investigation shows that the midlatitude MSTIDs can influence the F region plasma processes even over very low latitudes under favorable background conditions.

Plain Language Summary Medium-scale traveling ionospheric disturbances (MSTIDs) generated in the midlatitude are found to propagate toward the equator. While crossing the equatorial ionization anomaly crest region most of these structures dissipate due to ion drag. A deep ingression of the MSTID to a very low geomagnetic latitude (near to the geomagnetic equator) over the Indian sector is noted during the descending phase of the 24th solar cycle. Weak and asymmetric equatorial ionization anomaly formation is believed to support the deep ingression processes. On the observational night quasiperiodic southward moving waves and a small-scale southward moving wave signature are also observed in addition with the MSTID. The dissipation of all these features is possibly due to existence of the midnight pressure bulge. Present study provides an observational evidence of the midlatitude MSTID propagation into the low latitudes and their interaction with the low-latitude ionospheric/thermospheric processes, for example, midnight pressure bulge.

1. Introduction

The fundamental properties of the gravity waves and their relationship with traveling ionospheric disturbances (TIDs) were reported by Hines (1960). Since then, several reviews illustrated the extensive research carried out on this topic (e.g., Francis, 1974; Hocke & Schlegel, 1996; Hunsucker, 1982). The TIDs are considered as ionospheric manifestations of the atmospheric gravity waves generated in the middle and lower atmosphere by various sources such as thunderstorm, cyclone, and auroral joule heating. Based on the scale size TIDs are broadly classified into two categories: (1) large-scale TIDs (LSTIDs) and (2) medium-scale TIDs (MSTIDs). LSTIDs have larger horizontal wavelengths ($\geq 1,000$ km), longer periods (30 min to 3 hr), and higher phase speeds (400–1,000 m/s) compared to MSTIDs. In case of MSTIDs the phase speeds are ~ 50 –500 m/s, horizontal wavelengths ~ 100 –1,000 km, and period ~ 15 –90 min (Francis, 1974; Hunsucker, 1982). It is believed that the LSTIDs originate in the high-latitude ionosphere owing to the auroral energy input and MSTIDs are mostly generated in the midlatitude by the lower atmospheric gravity waves (e.g., Kelley, 2011; MacDougall et al., 2009; Moffett & Balthazor, 1997; Röttger, 1977).

Earlier, Shiokawa et al. (2002) reported the low-latitude extent of the midlatitude MSTID to be $\sim 18^\circ$ magnetic latitude (MLAT). Later on, Narayanan et al. (2014) showed that the MSTIDs could reach even below 13° MLAT in the absence of equatorial ionization anomaly (EIA) crest and midnight brightness waves (MBWs). Detection of the MSTIDs over a low-latitude station can provide critical missing links for the understanding of the characteristics of these MSTIDs and background conditions that favor these MSTIDs to reach very low latitudes.

Based on the Global Positioning System-total electron content (GPS-TEC) and radar measurements (Grocott et al., 2013; He et al., 2004; Hernández-Pajares et al., 2006; Jonah et al., 2017), it is now well accepted that the MSTIDs can occur during both day and night and their generation mechanisms can be different (Kotake et al., 2007; Tsugawa et al., 2007). The daytime MSTIDs propagate toward south-east in the northern hemisphere (Kotake et al., 2007). The unique feature of the nighttime MSTID is that north-west (NW) to south-east (SE) aligned phase fronts with south-westward propagation in the northern hemisphere (north-east [NE] to south-west [SW] aligned phase fronts with north-westward propagation in southern hemisphere; Otsuka et al., 2013; Shiokawa, Ihara, et al., 2003). The electric fields associated with the nighttime MSTIDs have also been observed by radar and in situ measurements (Saito et al., 1995; Shiokawa, Otsuka, et al., 2003). Earlier investigations suggested that gravity waves are responsible for the generation of daytime MSTIDs through ion-neutral collisions (Kotake et al., 2006, 2007; Kubota et al., 2011; Otsuka et al., 2013). However, this mechanism cannot explain the azimuthal alignments of nighttime MSTIDs. Thus, the source of the nighttime MSTIDs was conventionally believed to be associated with the Perkins instability process in the midlatitude ionosphere.

Perkins (1973) pointed out that the nighttime midlatitude F layer equilibrium could be supported by the southward wind or eastward electric fields against gravity, and the additional eastward winds or northward electric fields would promote the unstable condition. Although the phase alignments of the MSTIDs are consistent with the Perkins instability, it could not explain the equatorward-westward propagation of the MSTIDs. According to this theory, the instability should propagate at the same velocity as the background $E \times B$ drift, which is almost always to the east (Garcia et al., 2000). Another discrepancy of this theory is that its growth rate is too small (in the order of $10^{-4}/s$) to account for the observations (Chou et al., 2017; Kelley & Makela, 2001; Makela & Otsuka, 2012). This arises a question regarding the exact mechanism that leads to the generation of nighttime MSTIDs.

Tsunoda and Cosgrove (2001) reported that formation of the sporadic E (E_s) layer in the midlatitude and their associated Hall current-driven polarization electric fields mapping to the F region could effectively enhance the polarization electric fields and plasma density perturbations leading to the development of the MSTIDs. The E_s layer instability mechanism envisages polarization electric field oscillation or $E \times B$ drift oscillation in the NW-SE direction, and such oscillations have been perceived (Otsuka et al., 2007; Saito et al., 2007). Furthermore, Cosgrove et al. (2004) showed that the growth rate of the instability in the coupled E_s layer and F region exceeds that of the Perkins instability acting alone. In addition, tidal theory suggests that the wind direction in the E_s layer would be southward. Therefore, through ion-neutral collision, the E_s layer would move southward. When the electric fields map between the E and F regions, the F region plasma structures follow the E_s layer movement so that the MSTIDs with NW-SE phase front propagate south-westward (Makela & Otsuka, 2012). However, observational evidence of E - F region coupling processes are limited (Otsuka et al., 2007; Saito et al., 2007) and this aspect requires consolidation with more observations.

Previous studies revealed several characteristics of the MSTIDs from various locations (Candido et al., 2008; Duly et al., 2013; Fukushima et al., 2012; Kotake et al., 2006, 2007; Kubota et al., 2011; Martinis et al., 2010; Narayanan et al., 2014; Negrea et al., 2018; Otsuka et al., 2013; Shiokawa, Ihara, et al., 2003; Tsugawa et al., 2007). From these studies it is clear that the nighttime MSTIDs are more active during June solstice over Japan (Shiokawa, Ihara, et al., 2003) and Australian sectors, whereas it is more active during December solstice over the European sector (Kotake et al., 2006). Earlier reports showed that the nighttime MSTID occurrences were solar cycle dependent, that is, the occurrence rate is more during solar minimum and less during the solar maximum (Candido et al., 2008; Martinis et al., 2010; Narayanan et al., 2014).

It is shown that the MSTIDs appear over magnetically conjugate locations (Martinis et al., 2011; Otsuka et al., 2004; Shiokawa et al., 2005; Valladares & Sheehan, 2016). Duly et al. (2013) reported that the

MSTIDs are present in the midlatitude F region about 20–68% (equinox-solstices) of the time and these could reach low-latitude region. Makela et al. (2010) showed that during solar minimum period, MSTIDs could reach to the low latitudes. In addition, Miller et al. (1997) and Krall et al. (2011) suggested that MSTIDs could serve as seed perturbations for equatorial plasma bubbles (EPBs) and midlatitude spread F . Further, Otsuka et al. (2012) reported that the interaction between an MSTID and an EPB could cause the dissipation/disappearance of the EPB.

Most of the midlatitude MSTIDs reported earlier were either detected over midlatitude itself or closer to the low-latitude and midlatitude transition zone. The detection of midlatitude MSTIDs over very low latitudes (closer to the equatorial region) is sparse (Makela et al., 2010). Paulino et al. (2016) presented a statistical report on periodic waves in the thermosphere over Brazilian equatorial latitudes. Recently, Sau et al. (2018) reported the occurrence of quasiperiodic waves and single band of enhanced intensity over an equatorial station, Tirunelveli. However, they did not find any prominent signature of MSTID. To the best of our knowledge, there is only available study that reported the nighttime MSTID at a latitude as low as 5° MLAT during solar minimum condition (Makela et al., 2010). The present study provides an observational evidence of the midlatitude MSITD ingress even into a lower latitude ($\sim 3.5^\circ$ MLAT) for the first time. The possible background conditions that facilitate this deep ingress are discussed. Further, signatures of the quasiperiodic southward moving waves (QPSMWs) over the same station on the same night are also shown.

2. Instrumentation and Data Analysis

2.1. All-Sky Airglow Imagers

To study the mesosphere-thermosphere/ionosphere dynamics and coupling processes, an all-sky airglow imager is operated at the National Atmospheric Research Laboratory (NARL), Gadanki (13.5°N , 79.2°E ; $\sim 6.6^\circ$ MLAT), a low-latitude Indian station. This imager has three filters, viz., a wideband OH filter notched at 865 nm and two narrow band filters: 557.7 nm (for OI 557.7-nm emission) and 630 nm (for OI 630-nm emission). The filters are used to measure the mesospheric hydroxyl airglow (peaks ~ 85 km), mesospheric atomic oxygen (O^1S), and thermospheric atomic oxygen (O^1D) emissions. The exposure times for the images used for the present study are 15, 110, and 110 s for 865, 557.7, and 630-nm channels, respectively. The temporal resolution of the airglow images is 4 min. The front-end optics of the imager consists of a fish-eye lens with 180° full field of view (FOV; effective FOV $\sim 117^\circ$), followed by collimating lens, filter chamber, imaging lens, and a charge coupled device. During the operation, the charge coupled device temperature is maintained at -70°C temperature and the filter chamber is maintained at $\sim 25^\circ\text{C}$ in accordance with the transmission peak of the filters. Detailed description of the all-sky imager is available elsewhere (Taori et al., 2013). To characterize the thermospheric/ionospheric MSTID event reported in the present work, OI 630-nm airglow emission data have been utilized. With the present FOV ($\sim 117^\circ$), the images cover an area of $\sim 600 \times 600$ km (corresponding latitude and longitude $\sim 10.5\text{--}16.5^\circ\text{N}$, $76\text{--}82^\circ\text{E}$; $\sim 3.3\text{--}10^\circ$ MLAT) at the OI 630-nm peak emission altitude of 250 km. Therefore, the 630-nm airglow image can track the MSTIDs as low as $\sim 3.5^\circ$ MLAT.

In order to ascertain the MSTID event under consideration, additional observations from the airglow imager at Allahabad (25.5°N , 81.9°E ; MLAT $\sim 16.30^\circ\text{N}$), a low-latitude station closer to the crest region of the equatorial plasma fountain (or the crest region of EIA), are also used. The optical design of the airglow imager at Allahabad is similar to that of the NARL airglow imager except the number of filter channels. Allahabad imager contains six interference filters in its filter chamber, viz., OI 630 nm (peaks ~ 250 km), OI 557.7 nm (peaks ~ 97 km), 840 nm, 846 nm (molecular oxygen emission, peaks ~ 94 km), and OH Meinel bands at 720–910 nm with notch at 850–870 nm (peaks ~ 85 km) and an 857-nm filter for background light. The details of this imager are also available elsewhere (Parihar et al., 2018).

To identify the presence of the wave signatures in the OI 630-nm images, the acquired raw images are unwrapped and projected onto an equidistant grid. All projected images (image at a particular time is denoted by $I(t)$) on a given night are averaged to obtain a nightly averaged image or mean image (I_m). To obtain the residual intensity variation (I_r), the image at a given time is subtracted from the nightly mean image ($I_r = I(t) - I_m$). To doubly verify, the residual images are also compared with the original projected images and it is found that the residual images do not show any notable difference in the wave structures

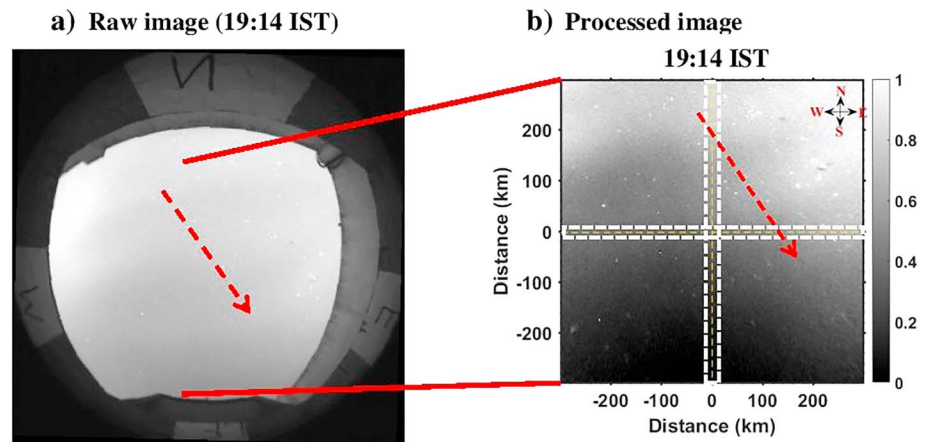


Figure 1. Sample images of OI 630-nm emission: (a) raw image and (b) processed image (19:14 Indian Standard Time [IST]); the centers of these images imply the observational location (i.e., Gadanki). In Figure 1b x and y axes denote image covering area in zonal (east-west) and meridional (north-south) direction around OI 630-nm emission altitude (i.e., ~250 km). The center is located at the intersection of vertical and horizontal dashed yellow lines that were marked at 0 km, and the white dotted region implies the portion that is taken for east west and north south keogram. In these figures the red dotted arrow implies the quasiperiodic southward moving wave signature.

except the background intensity variations. The method adopted to estimate the wave parameters based on these images is further elaborated in section 4.

Figure 1 shows samples of OI 630-nm raw image (Figure 1a) and processed image (Figure 1b), respectively. In Figure 1b x and y axes indicate image covering area in zonal (east-west) and meridional (north-south) directions around OI 630-nm emission altitude (i.e., ~250 km). The centers of these images denote the observational location (i.e., Gadanki). The center is located at the intersection of vertical and horizontal dashed yellow lines that were marked at 0 km (location of Gadanki). Northward and eastward directions are considered positive in this figure. The red dotted arrow represents the propagation of a wave toward south-east direction that can be discerned from the processed image. In order to construct a keogram, the image data obtained from Gadanki are further analyzed to construct east-west (EW) keograms (fixed latitude with varying longitudes) and north-south (NS) keograms (fixed longitude with varying latitudes). The part of the image enclosed by the white dotted lines (Figure 1b) is used to construct the keograms (averaged over three pixels).

3. Results

3.1. Medium Scale Traveling Ionospheric Disturbances (MSTID)

The wave signatures with north-west (NW) to south-east (SE) aligned phase fronts moving south-west (SW) are observed in the OI 630-nm airglow emission images over a low-latitude station Gadanki, on 12 January 2016 during 16:41–17:34 UT (22:11–23:04 Indian Standard Time [IST]). Note that universal time (UT) and IST are related by $IST = UT + 5.5 \text{ hr}$ (hereafter IST is used). An example of four consecutive OI 630-nm airglow images from 22:30 IST to 22:42 IST with NW to SE aligned phase front is shown in Figure 2. These signatures are considered to be related to the passage of the MSTID over Gadanki because the observed characteristics such as horizontal wavelength, horizontal phase velocity, period, and propagation direction of the wave event are consistent with those of MSTIDs (discussed in the ensuing paragraphs). In Figure 2 x and y axes are the same as Figure 1b. Figure 2 reveals two distinctly different dynamical features. One, the MSTIDs feature those phase fronts aligned in the NW to SE direction and propagating in the SW direction their phase front alignment highlighted by red lines and propagation direction highlighted by red arrows. Second, EW phase front aligned QPSMWs, which appears in the SE part of the images that is discussed in section 3.2. Figure 2 clearly show the phase propagation of the MSTID and QPSMW, and this also shows the decrease in the intensity of QPSMW with time.

In this analysis, correlation coefficients are not calculated for an appropriate lag in a conventional method. Instead, the MSTID parameters are derived based on image analyses. The distance between peak (maxima)

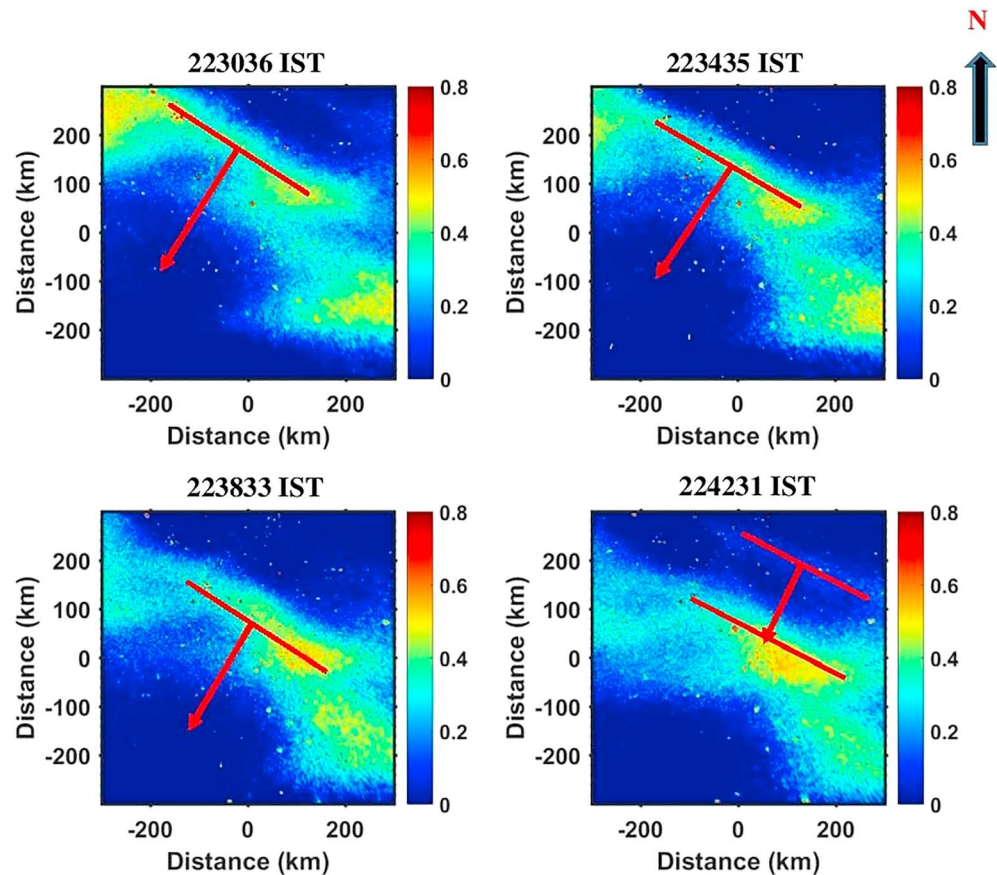


Figure 2. Consecutive images of north-west to south-east aligned phase fronts with south-westward moving wave signature in the OI 630-nm airglow images over Gadanki from 22:30 Indian Standard Time (IST) to 22:42 IST. In these images phase fronts are heightened by the red line and the phase propagation is represented by the red arrow. In these images upper side denotes the north, and right side denotes the east direction from the observational location (i.e., Gadanki). In addition to the medium-scale traveling ionospheric disturbance, EW aligned phase fronts also evident in the south-eastern part of these images are representative of quasiperiodic southward moving waves.

of two phase fronts on a given image (along the phase propagation direction) is considered as wavelength, wherein the temporal evolution of the positions of the phase fronts from the given image to the successive image provides phase velocity. For example, if the position of the wave phase (identified by intensity maxima) is (x_1, y_1) in the first image and in the successive image, the corresponding position is (x_2, y_2) and the horizontal displacement is $S = \sqrt{(x_2 - x_1)^2 + (y_2 - y_1)^2}$. As the time difference between two consecutive images is 4 min (i.e., time resolution of the observation) for the present case, the horizontal phase velocity is obtained by dividing horizontal displacement with the time difference, that is, $V_p = S / (4 * 60)$. In graphical method, to deduce the horizontal wavelength, the intensities along the wave propagation direction (perpendicular to the phase fronts) are plotted with distance. The distance between two maxima (minima) provides the horizontal wavelength. Similarly, the horizontal phase velocity is calculated using phase difference that is calculated from the line intensity plots of consecutive images. Using the horizontal wavelength and horizontal phase velocity, period of the MSTID is calculated. Manually and graphically derived MSITD parameters are given in Table 1.

The horizontal wavelength, horizontal phase velocity, and period of the MSTID are found to be 160 ± 6 (175 ± 1) km, 138 ± 14 (130 ± 6) m/s, and 19.5 ± 3 (22 ± 0.4) min, respectively, wherein the numbers outside and within parentheses denote the manually and graphically derived values, respectively. The characteristics of this MSTID is consistent with the earlier investigation by Taori et al. (2015), and the observations of this MSTID over Gadanki, which is at 6.6° MLAT and the FOV covers as low as $\sim 3.5^\circ$ MLAT, make it special.

Table 1
Parameters of the Observed Wave Events (MSTID, QPSMW, and SSSMW)

Event	Observation interval IST	Horizontal wavelength (km)	Phase velocity (m/s)	Period (min)	Propagation direction and angle
MSTID Over Gadanki	22:11–23:04	160 ± 6 or (175 ± 1)	138 ± 14 or (130 ± 6)	19.5 ± 3 or (22 ± 0.4)	South-westward ($\sim 235^\circ \pm 1^\circ$)
Over Allahabad	18:44–19:40	106.8 ± 11	139 ± 26	13.7 ± 2.39	South-westward ($\sim 258^\circ \pm 4^\circ$)
QPSMW	19:30–23:00	367 ± 14	131 ± 18	46.7 ± 13	South-east ($142.6^\circ \pm 4^\circ$) and south ($\sim 180^\circ$)
SSSMW	21:01–22:46	157 ± 4	121 ± 18	21.7 ± 3.4	Southward ($\sim 180^\circ$)

Note. The parameters in brackets denote the graphically derived values. Indian Standard Time, IST; Medium-scale traveling ionospheric disturbance, MSTID; quasiperiodic southward moving wave, QPSMW; small-scale southward moving wave, SSSMW.

3.2. Quasi-Periodic Southward Moving Waves (QPSMW)

QPSMW are commonly observed features in the OI 630-nm airglow images, near the dip equatorial region. These waves have primarily EW phase fronts and propagate southward with a velocity of 310 ± 110 m/s and a period of 40 ± 15 min (Shiokawa et al., 2006). Interestingly, QPSMW is observed over Gadanki during 19:30–23:00 IST on the same night (i.e., 12 January 2016) before the arrival of MSTID over this latitude.

In order to visualize the spatial and temporal evolution of the QPSMW, keograms are constructed using normalized and residual airglow emission intensities, which are shown in Figures 3a–3d. Figures 3a and 3b show the EW and NS keograms in terms of normalized intensity, and Figures 3c and 3d show the EW and NS keograms in terms of residual intensity. In these Figures 3a–3d x axis denotes the time (IST) and y axis denotes the distance (km) in the zonal (EW; Figures 3a and 3c) and meridional (NS; Figures 3b and 3d) directions. In general, the QPSMW phase fronts are aligned in the EW direction, as clearly visible in the EW keogram (Figures 3a and 3c), and NS keograms clearly show the southward propagation of the phase fronts highlighted by the red dotted arrows. Initially, the wave structures move toward south-east (not visible in keogram). Later on, the direction of propagation of the wave changes to southward. As mentioned in the previous section on this night MSTID signature is also observed. However, the intensity variation due to QPSMW is stronger than that caused by the MSTID, and therefore, the QPSMW signature dominates the

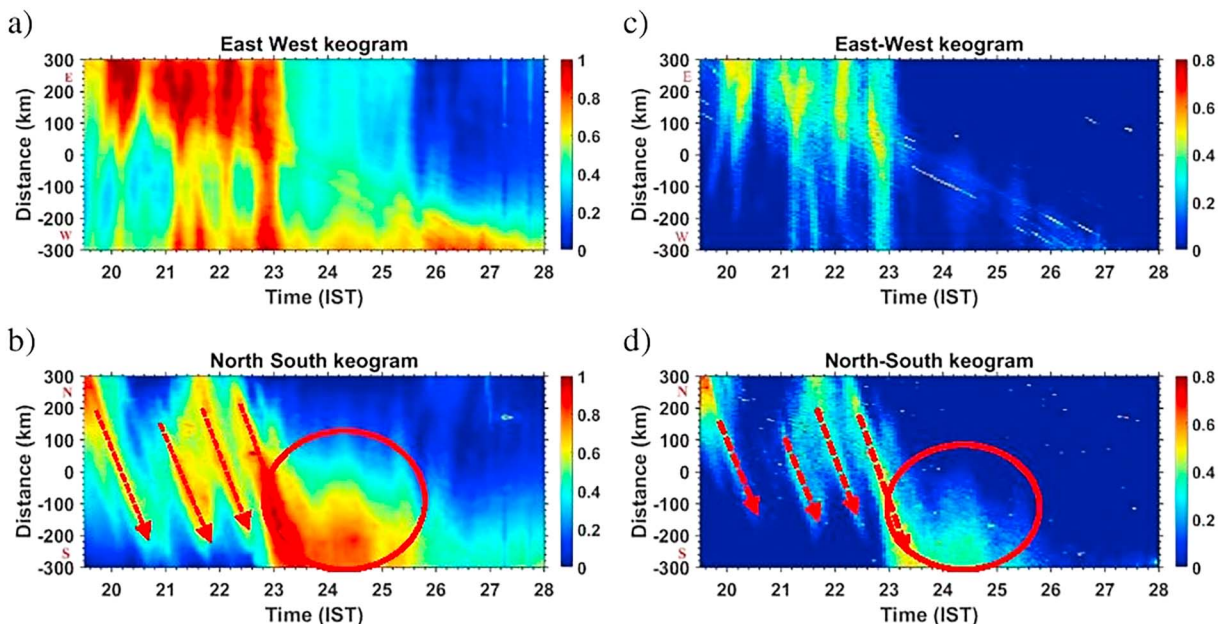


Figure 3. (a) EW keogram of OI 630-nm normalized airglow emission intensity, (b) NS keogram of OI 630-nm normalized airglow emission intensity, (c) EW keogram of residual intensity, and (d) NS keogram of residual intensity. In these figures (a–d) x axis denotes the time (Indian Standard Time [IST]) and y axis denotes the distance (km) in the zonal (EW; Figures 3a and 3c) and meridional (NS; Figures 3b and 3d) directions. EW keogram clearly indicates the phase front alignment parallel to the EW direction, and the NS keogram shows the southward phase propagation that is highlighted by red dotted arrows. Further, NS keogram also shows the midnight OI 630-nm emission intensity enhancement in the southern side of Gadanki that is highlighted by red circle.

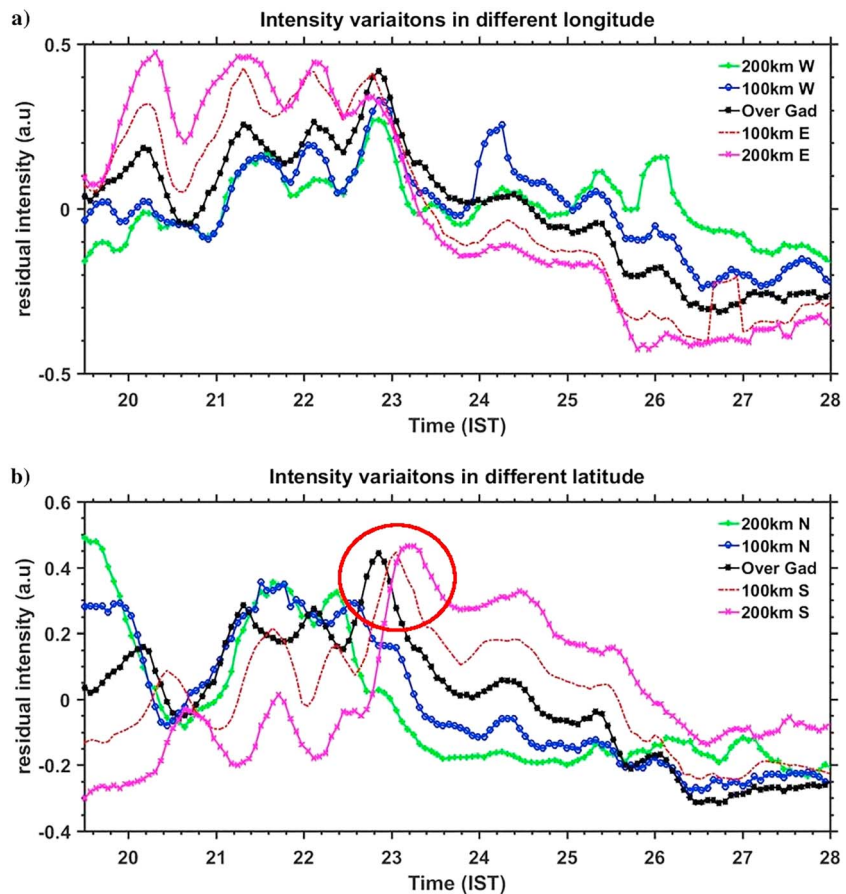


Figure 4. Spatial (latitudinal and longitudinal) and temporal variation of OI 630-nm airglow emission intensity. (a) Intensity variation at 200 km (green line) and 100 km (blue line) west of Gadanki, over Gadanki (black line), 100 km (red dotted line), and 200 km (pink line) east of Gadanki, respectively (taken from EW keogram for different longitude). (b) Intensity variation at 200 km (green line) and 100 km (blue line) north of Gadanki, over Gadanki (black line), 100 km (red dotted line) and 200 km (pink line) south of Gadanki respectively (taken from NS keogram- for different latitude). In these figures x axis denotes the time and y axis denotes the residual intensity. From Figure 4a it is clear that all the longitude intensity decreases with time after midnight though there is feeble east west asymmetry in intensity. Figure 4b clearly shows that there is a large north-south asymmetry in the emission intensity and also there is an enhancement during midnight in southern part of the images that is highlighted by a red circle.

keograms. Further, midnight intensity enhancement (marked by red circle) noted in the NS keogram (Figures 3b and 3d) is considered to be midnight pressure bulge (MPB) or midnight temperature maximum (MTM) that will be discussed in section 3.3.

The phase velocity of the QPSMW derived from the NS keogram comes out to be $\sim 131 \pm 18$ m/s. Note that the time delays are derived from the keogram based on the separation between two points along the same phase. The phase fronts are highlighted by the red dotted arrows. As along any given arrow, multiple phase speeds can be calculated by taking different sets of points; an average phase velocity is determined. Further, to calculate the periodicity, intensity variations (taken from the keogram) are plotted with latitude and longitude that is presented in Figure 4. In Figures 4a and 4b x axis denotes the time and y axis denotes the residual intensity. Figure 4a show the intensity variation at 200 km (green line), 100 km (blue line) west of Gadanki, over Gadanki (black line), 100 km (red dotted line), and 200 km (pink line) east of Gadanki respectively (generated from EW keogram for different longitude) with time. Figure 4b describes the intensity variation similar to Figure 4a but for different latitude (i.e., generated from NS keogram) that will be detailed in section 3.3. All the longitudes show similar oscillations with feeble east west asymmetry in the emission intensity, and this figure also depict that in all the longitudes after midnight intensity decreases with time. From the intensity variation, the QPSMW period is calculated using Lomb-Scargle Periodogram (LSP), which comes out to

be $\sim 46.7 \pm 13$ min. The horizontal wavelength of the QPSMW deduced from the horizontal phase velocity and period (wavelength = phase velocity \times period) is found to be $\sim 367 \pm 14$ km. The QPSMW signature was observed in the images up to 23:00 IST after that it disappeared in the keogram. However, the QPSMW signatures are also present during postmidnight hours, albeit with smaller amplitudes as seen in Figure 4.

3.3. Midnight Pressure Bulge/Midnight Temperature Maximum (MPB/MTM)

On this night, enhancement in the airglow emission intensity is observed around midnight (started at $\sim 23:00$ IST) in the southern part of the observational location that can be clearly seen in Figures 3b and 3d (NS keogram) highlighted by red circle. These enhancements are probably associated with MTM or MPB. The meridional extension of the intensity enhancement is noticed up to Gadanki until $\sim 26:00$ (02:00) IST, that is clearly visible in Figure 4b as well (intensity variation at different latitude with time), and this figure also depict a clear north south asymmetry in the emission intensity. In the northern latitudes of the observational location intensity decreases with time, however, in southern latitudes intensity increases with time and the maximum intensity enhancement is observed during midnight (as shown in Figure 4b, red circle) after that it decreases with time.

The winds generated due to MPB at the equator propagate poleward (northward), and its vertical component pushes the *F* region plasma downward causing a region of enhanced airglow production (Mukherjee et al., 2006). Due to the descent of the *F* layer, the electron density in the airglow emission altitude/bottom of the *F* layer also increases.

3.4. Small-Scale Southward Moving Wave (SSSMW)

In addition to the above mentioned features, a small-scale southward moving wave (SSSMW) signature is also noted from 21:01 IST to 22:46 IST. Figure 5a show sequence of a few SSSMW images from 21:07 to 21:19 IST. In these images *x* and *y* axes are the same as Figure 1b. On the east side of these images QPSMW feature can be noted. On the west side of these images, two faint bands propagating southward can be noted. Although the propagation direction of these wavefronts is similar to the QPSMW, their wave characteristics are different. Intensity variations along the wave propagation for a few images are shown in Figure 5b (taken from 200 km west of Gadanki as indicated by red dotted lines in Figure 5a) that clearly identify southward phase propagation. In Figure 5b, *x* axis represents the distance in north south direction and the red dotted arrows represent the phase propagation. The horizontal wavelength, horizontal phase velocity, and period of the wave are estimated to be $\sim 157 \pm 4$ km, $\sim 121 \pm 17.8$ m/s, and $\sim 21.7 \pm 3.4$ min, respectively. It is clear that wavelength and period of this wave feature are smaller than the QPSMW. Thus, this feature is considered as a SSSMW in the present study. Details of the MSTID, QPSMW and SSSMW parameters are provided in Table 1.

4. Discussion

The present work highlights the presence of multiple nocturnal dynamic features (viz., MSTID, QPSMW, MTM/MPB, and SSSMW) that are noted on a single night over a low-latitude station Gadanki. Interaction between these processes and their possible dissipation mechanisms are discussed below.

EPB, one of the important phenomena occurring in the low-latitude ionosphere, can be easily detected in the OI 630-nm airglow emissions. It is well known that the EPB depletions are aligned parallel to the magnetic field (north-south) and drifts either from west to eastward (mostly) or east to westward (rarely). The present study deals with the OI 630-nm airglow depletions having EW phase front alignment and propagates meridionally. Therefore, these features are obviously not associated with EPBs.

The south-westward moving wave signatures with NW to SE aligned phase fronts are observed around 22:11 IST in OI 630-nm airglow images. These features are associated with MSTIDs as all the characteristic features are consistent (Shiokawa, Ihara, et al., 2003; Otsuka et al., 2013; Narayanan et al., 2014) with the MSTID features. In order to ascertain further, OI 630-nm airglow images from an off-equatorial station, Allahabad, are looked into. The images from Allahabad show similar kind of wave features moving south-westward with a phase velocity of 139 ± 26 m/s. These features are perceived in the Allahabad OI 630-nm images from 18:44 IST onward and continued till 19:40 IST (approximately almost an hour) as shown in Figure 6. The projected distance between Gadanki and Allahabad along the MSTID propagation direction

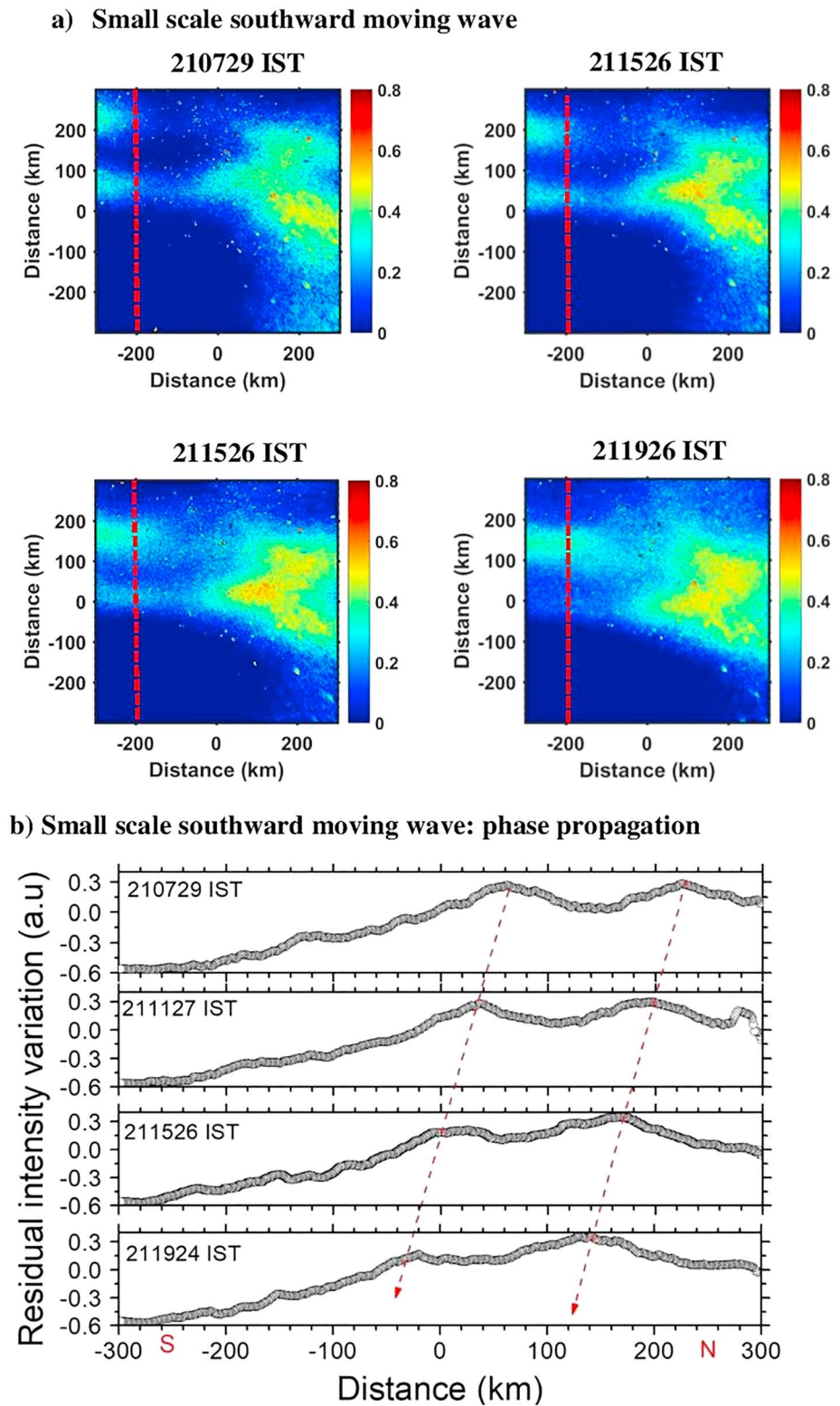


Figure 5. (a) Sequence of few small-scale southward moving wave images from 21:07 to 21:19 Indian Standard Time (IST); in these images x and y axes are the same as Figure 1b. These images clearly show two east-west phase fronts that are propagates toward south. (b) Phase propagation of the small-scale southward moving wave event; the intensity variations are taken from 200 km west of Gadanki (as indicated by red dotted lines in Figure 5a). In Figure 5b x axis represents the distance in north south direction, y axis denotes the residual intensity variation, and the red dotted arrows represent the southward phase propagation.

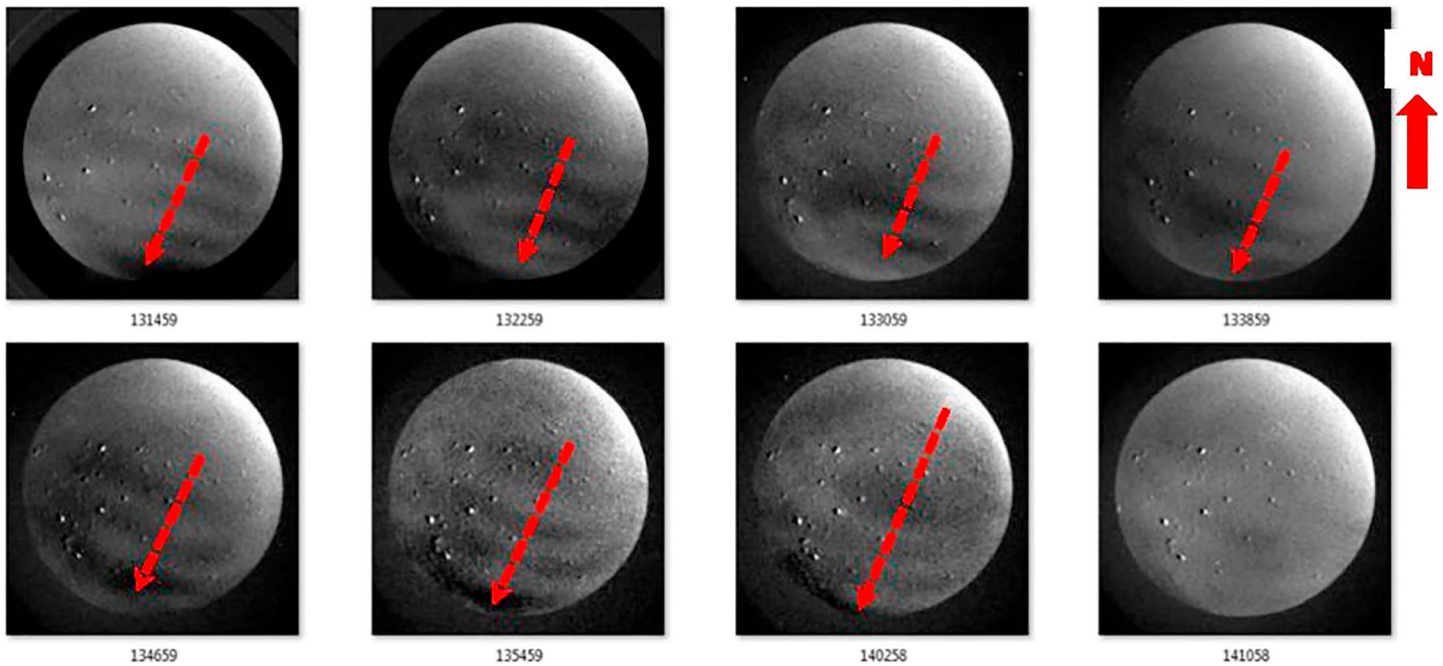


Figure 6. Medium-scale traveling ionospheric disturbance signature over Allahabad (an off-equatorial station) on 12 January 2016 during 18:44 Indian Standard Time (IST) to 19:40 IST. Medium-scale traveling ionospheric disturbance propagation direction is indicated by the red dotted arrow.

is $\sim 1,372$ km. If the MSTID observed at Allahabad is assumed to propagate with the above mentioned constant phase velocity, it should take ~ 3 hr to reach Gadanki. The observed time delay between the appearance of MSTIDs over the two stations is found to be ~ 3.5 hr (the MSTID starts appearing over Gadanki at 22:11 IST). This increase in the time delay is expected as the MSTID may not move with a constant phase velocity and can slow down due to the finite ion drag present during post sunset hours over the low-latitude region. Nevertheless, this reasonable consistency in the time delay between the two low-latitude stations reconfirms that the MSTID that is observed over Gadanki appeared over Allahabad 3.5 hr earlier on this night. Interestingly, the duration of MSTID appearance over both the stations is close to 1 hr. While over Gadanki, the duration of MSTID propagation is 22:11–23:04 IST; it is 18:44–19:40 IST over Allahabad. This additionally confirms the propagation of the MSTID from Allahabad to Gadanki and suggests a very deep ingress of MSTID into low latitudes on this night.

Earlier, using the observations of GPS-TEC and OI 630-nm airglow imaging, Shiokawa et al. (2002) reported that the equatorial limit of MSTID is $\sim 18^\circ$ MLAT. They argued that the presence of the crest of EIA (EIA peaks around $\sim 20^\circ$ MLAT; Balan et al., 2018) constrained the deep ingress of MSTID to very low latitudes. An enhanced EIA increases the electron density in the crest region that in turn increases the ion drag and dissipates the MSTID. Narayanan et al. (2014) showed the presence of MSTIDs throughout the night despite the presence of EIA crests in the postsunset hours. Thus, EIA alone cannot be considered to be a sole factor for disappearance of MSTIDs. At the same time, poleward propagating MBW in association with MPB can also be a potential limiting factor for the equatorward propagation of the MSTIDs. Narayanan et al. (2014) suggested that the nighttime MSTIDs could disappear due to the perturbations associated with MPB like MBW or due to the existence of the strong EIA crest region. Therefore, in the absence of such features, the MSTIDs are supposed to reach very low latitudes.

To understand the possible strength of the EIA crest after sunset, the hourly average Global Navigation Satellite System (GNSS) TEC maps are investigated. Figures 7a and 7b show the global TEC variation at 18:30 IST and 19:30 IST, wherein the TEC variations over the Indian sector is zoomed in and shown on the right side, and the OI 630-nm airglow observational locations are indicated by the star symbols. It is clear from the TEC maps that the daytime EIA crests are significantly asymmetric during 18:30–19:30 IST. Not only the latitudinal width of the northern crest significantly narrower compared to the southern crest but also the northern crest is closer to the dip equator as compared to the southern crest. Therefore, during

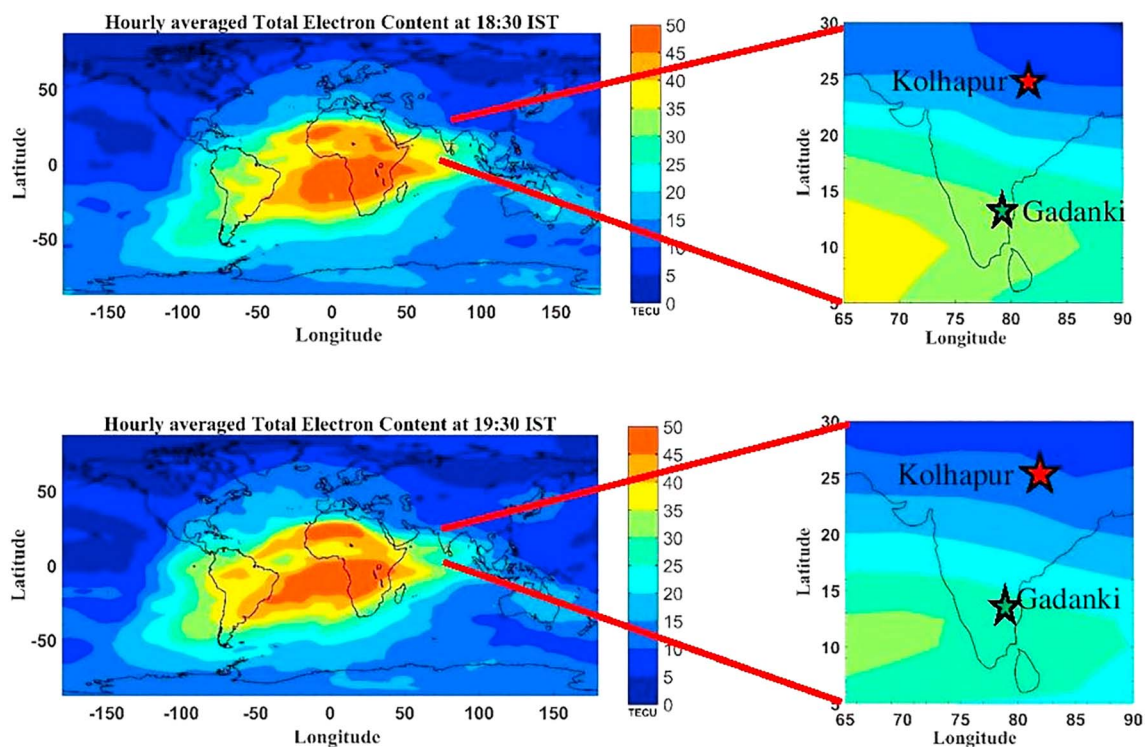
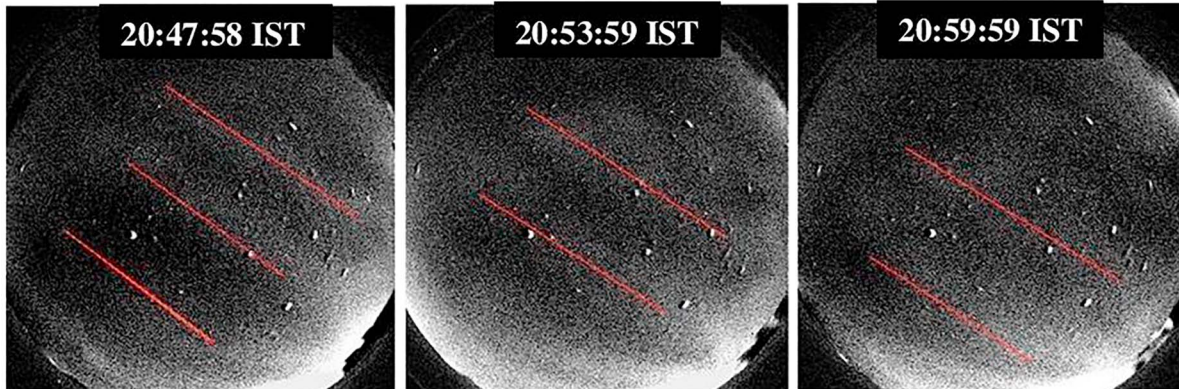


Figure 7. (a and b) Hourly averaged Global International Global Navigation Satellite System (GNSS) Service total electron content map on 12 January 2016 at 18:30 Indian Standard Time (IST) and 19:30 IST, respectively. The right hand side shows the zoomed-in Indian sector, and the stars in the zoomed portion represent the OI 630-nm airglow observation location. These figures clearly depict that the equatorial ionization anomaly is very weak and asymmetry over the Indian sector during the postsunset hours.

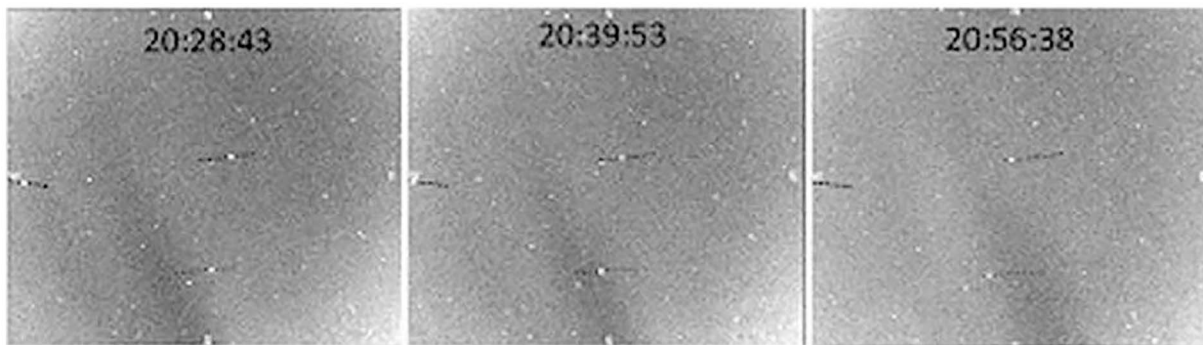
postsunset hours, the depleted (see the zoomed-in figures) and latitudinally narrower northern crest can assumed to be much closer to the dip equator and may favor deep ingression of MSTID on this night. Previously, Taori et al. (2015) studied the triggering mechanism of the EPB using OI 630-nm airglow images from three stations, viz., Gadanki, Kolhapur (16.8°N, 74.2°E), and Ranchi (23.3°N, 85.3°E; close to Allahabad) on 19 March 2012. During that night, Ranchi images show the MSTID signatures as shown in Figure 8a; Gadanki and Kolhapur images are revealed EPB signature as shown in Figures 8b and 8c (images used in Figure 8 is reproduced from Taori et al., 2015). With the help of these observations, additional verification is done to understand whether the absence of MSTID structure over Kolhapur and Gadanki on this night is due to the presence of the stronger EIA crest. In order to do this, global GNSS-TEC maps for 19 March 2012 at 18:30 IST and 17:30 IST are plotted in Figures 9a and 9b. The zoomed-in portion of the Indian sector is shown on the right side and the location of the observations is indicated by star symbols. Contrary to the present observation, the EIA crest over Indian sector is found to be very strong and more symmetric on this day and also during postsunset hours. This can be a possible reason for the absence of the MSTID over Kolhapur and Gadanki on 19 March 2012. Therefore, weak and asymmetric EIA crest on 12 January 2016 is believed to support the deep ingression of midlatitude MSTID to very low latitudes on this night. At the present moment, the inference is only suggestive and not quantitative. More observations (similar to the present study) are needed to show quantitatively the threshold TEC gradients over low latitudes that will hinder the ingression of MSTID to low latitudes. This will be taken up in future. In addition, since northward propagating wave structures associated with MBW feature are absent during midnight hours, the conditions are favorable for the MSTIDs to reach very low latitudes on this night.

Makela et al. (2010) showed that the MSTIDs could reach the low geomagnetic latitudes during low solar minimum period, because the EIA is generally very weak during the solar minimum period. However, the present observation is not carried out during solar minimum condition. The year 2016 is in the descending phase of the 24th solar cycle with sunspot number less than 40. Over Indonesian sector, Fukushima et al.

a) Ranchi OI 630 nm airglow images on 19 March 2012



b) Kolhapur OI 630 nm airglow images on 19 March 2012



c) Gadanki OI 630 nm airglow images on 19 March 2012

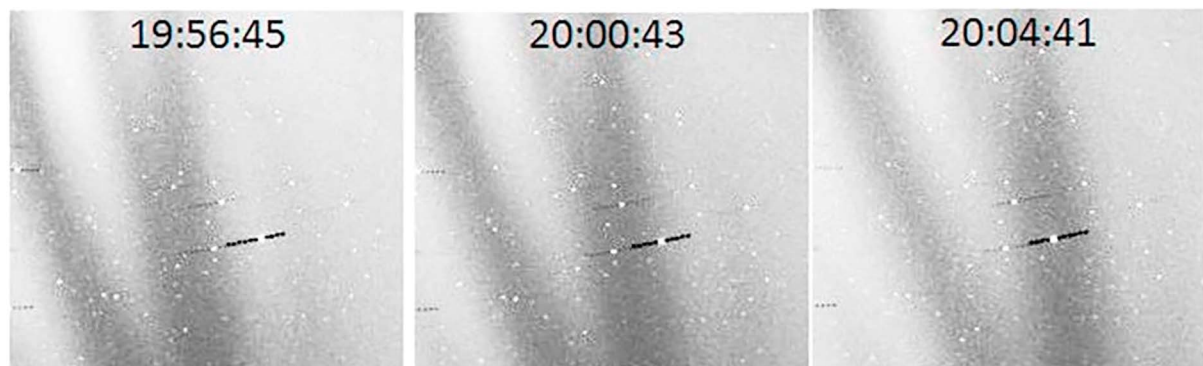


Figure 8. (a) Medium-scale traveling ionospheric disturbance over Ranchi. The red line denotes the medium-scale traveling ionospheric disturbance phase fronts. (b) Equatorial plasma bubble over Kolhapur and (c) equatorial plasma bubble over Gadanki. These images are taken from Taori et al. (2015).

(2012) studied the characteristics of *MSTIDs* using 7 years of airglow imager data. However, the characteristics are not similar to the midlatitude *MSTIDs*. The phase fronts of these *MSTIDs* were aligned in the east-west direction, and the occurrence was directly proportional to the solar cycle variation. It is generally accepted that midlatitude *MSTID* occurrence rate is more during solar minimum and less during solar maximum. Similarly, using 10 years (September 2000 to November 2010) of all-sky airglow imager data, Paulino et al. (2016) reported the statistical characteristics of the quasiperiodic waves over São João do Cariri, Brazil. According to this study, most of these waves are gravity waves rather than *MSTID*. Therefore, to the best of their knowledge, there was only one study (Makela et al., 2010) that reported the appearance of *MSTID* signature at low geomagnetic latitudes (up to 5° MLAT) over

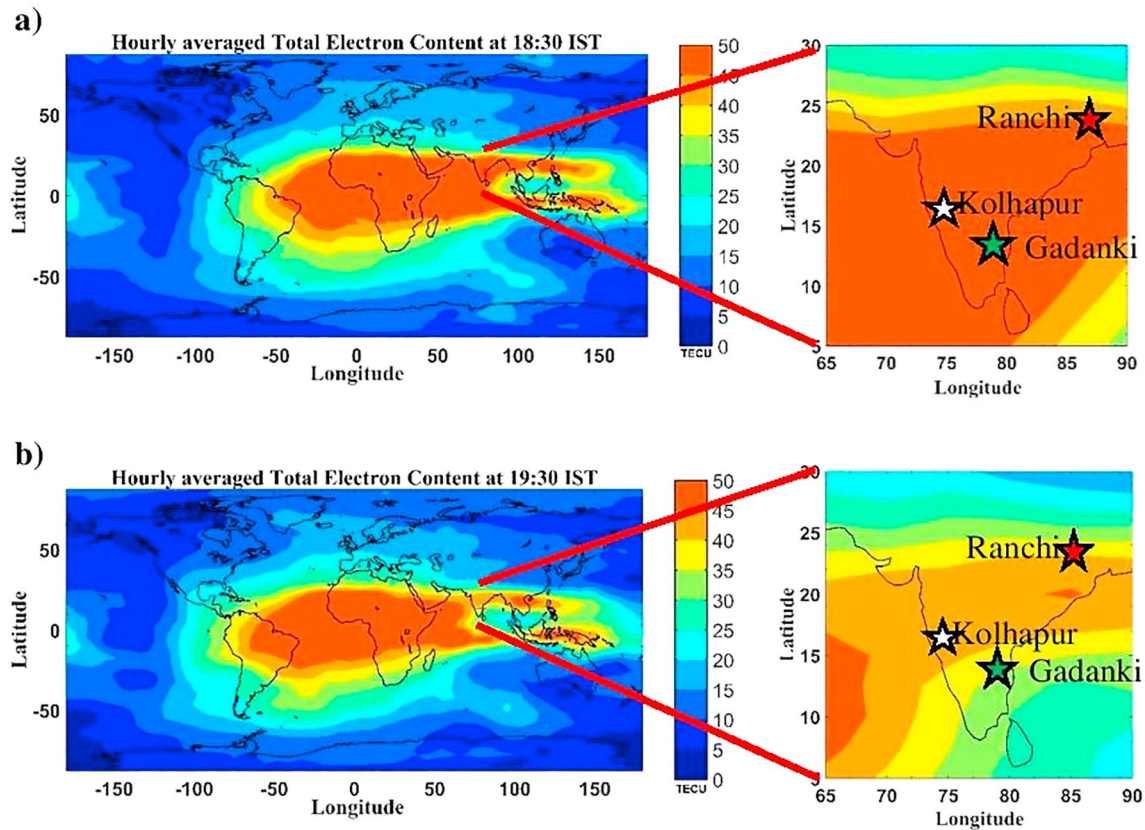


Figure 9. Same as Figure 7 but for 19 March 2012. These figures depict a strong and symmetric equatorial ionization anomaly structure over the Indian sector, and the equatorial ionization anomaly crest is located between Gadanki and Ranchi during the postsunset hours.

American sector. The present study shows the presence of the MSTID even lower MLAT ($\sim -3.5^\circ$) for the first time over the Indian sector.

The MSTID signature is seen in the OI 630-nm airglow images till 23:04 IST. Subsequently, there is an enhancement in the airglow emission intensity over the southern part (see Figures 3b and 3d and 4b as indicated by the red circles) of Gadanki starting at $\sim 23:00$ IST and it continues up to $\sim 26:00$ IST. One of the prime reasons for the midnight airglow emission intensity enhancement is the descent of the *F* layer, that is, increase of electron density in the airglow emission altitude (it is well known that the airglow emission intensity is proportional to the electron density and atomic oxygen density $O^+ + O_2 \rightarrow O_2^+ + O$; $O_2^+ + e^- \rightarrow O + O + \text{photons}$). Maruyama and Matuura (1984) reported that the bottomside electron density enhancements contribute to the increase in field-line integrated Pedersen conductivity. Such an enhancement in the conductivity might play a role in suppression of the polarization electric fields that are responsible for the sustenance of the nighttime MSTIDs (Kelley et al., 2000; Shiokawa, Otsuka, et al., 2003). Once the polarization electric fields vanish, the nighttime MSTIDs also disappear (Narayanan et al., 2014). Therefore, it can be inferred that MBW as suggested by Narayanan et al. (2014) or MPB as indicated in the present work can cause dissipation of MSTID over low-latitude region. This aspect requires more investigation with larger database.

As mentioned in the previous section, in addition to the MSTID a strong QPSMW structure from the post sunset to midnight is also observed in the present study. In the beginning, the wavefronts move toward southeast, later, the direction changes to southward, and the wave characteristics are consistent with the earlier reports (Sau et al., 2018; Shiokawa et al., 2006). While passing through the MPB these waves dissipate their energy significantly as seen in Figures 3b, 3d, and 4b. These figures also clearly show enhancement of intensity in the southern part and decrease in intensity in the northern part of the observational location after midnight. Neutral and electron density enhancement due to MPB can hinder the QPSMW propagation

that can be a prime reason for disappearance of QPSMW signature after midnight. However, the wavy structure remains visible in the line plots (see Figure 4b) with decrease in their amplitudes. It is evident that the MPB and associated neutral density enhancement could not suppress the QPSMW completely (considering large amplitude of the QPSMW). Previously, Shiokawa et al. (2006) suggested that the EIA expansion might be the origin of the QPSMW. However, during this night, the EIA crest is weak over the Indian subcontinent (see Figure 7). Therefore, further studies are required to verify whether QPSMW could be generated by some other sources in addition to the EIA.

In the present study, in addition to the MSTID and QPSMW features another wave feature (SSSMW) with propagation direction similar to QPSMW is noted. Although the propagation direction of the SSSMW is similar to the QPSMW, their characteristics such as horizontal wavelength, horizontal phase velocity, and period are found to be different. SSSMW phase fronts are detected in the images for more than one and half hour (21:01 IST to 22:46 IST). Another interesting factor is that SSSMW and QPSMW signatures are not observed in the Allahabad images and observed only in Gadanki images. This essentially means that these waves are generated somewhere between Gadanki and Allahabad. Interestingly, meteorological satellite cloud image data show deep convection between Gadanki and Allahabad (see the link <https://meteologix.com/br/satellite/india/top-alert-10min/20160112-2000z.html>). It suggests that these waves (QPSMW and SSSMW) might be generated by the lower atmospheric sources (i.e., convection) over low latitudes (Fukushima et al., 2012; Shiokawa et al., 2006).

5. Summary and Conclusions

Using OI 630-nm airglow observation, multiple thermospheric features such as MSTID, QPSMW, and MTM/MPB, SSSMW are observed on a single night (12 January 2016) over Gadanki, a low geomagnetic latitude station. The important results obtained from the present study are summarized below

1. A south-westward moving MSTID signature is identified very close to the dip equator. Imaging observations from Allahabad, a station close to the EIA crest, confirmed that the noted MSTID event was of mid-latitude origin and propagated to low latitudes. To the best of our knowledge, the present study reports the MSTID signature at a latitude as low as 3.5° MLAT for the first time.
2. It is shown that weak and asymmetric EIA crest on this night provided favorable background condition for the deep ingress of the midlatitude MSTID to very low latitudes. The absence of northward propagating MBW associated with MPB also assisted the deep ingress of MSTID on this night.
3. In course of propagation through the MPB, the MSTID structure disappeared. The physical reason behind the dissipation might be the MPB associated electron density enhancement at the bottom side of the F layer that increased the Pederson conductivity. The Pederson conductivity might suppress the polarization electric fields that were responsible for the sustenance of the nighttime MSTIDs.

In addition, a QPSMW signature was also observed during premidnight hours on this night. The NS keogram suggests that these structures disappeared while passing through the MPB. However, the QPSMW signatures are also present during postmidnight hours, albeit with smaller amplitudes. It is evident that the MPB and associated neutral density enhancement could not suppress the QPSMW completely (due to large amplitude of the QPSMW).

1. This study also suggests that the QPSMW could be generated by some other sources in addition to the EIA.
2. In addition to the above features, a SSSMW signature also noted during this night. Though the direction of propagation of this feature is similar to the QPSMWs, their characteristics are different.

References

- Balan, N., Souza, J., & Bailey, G. J. (2018). Recent developments in the understanding of equatorial ionization anomaly: A review. *Journal of Atmospheric and Solar - Terrestrial Physics*, 171(April 2017), 3–11. <https://doi.org/10.1016/j.jastp.2017.06.020>
- Candido, C. M. N., Pimenta, A. A., Bittencourt, J. A., & Becker-Guedes, F. (2008). Statistical analysis of the occurrence of medium-scale traveling ionospheric disturbances over Brazilian low latitudes using OI 630.0 nm emission all-sky images. *Geophysical Research Letters*, 35, L17105. <https://doi.org/10.1029/2008GL035043>
- Chou, M. Y., Lin, C. C. H., Yue, J., Tsai, H. F., Sun, Y. Y., Liu, J. Y., & Chen, C. H. (2017). Concentric traveling ionosphere disturbances triggered by Super Typhoon Meranti (2016). *Geophysical Research Letters*, 44, 1219–1226. <https://doi.org/10.1002/2016GL072205>

Acknowledgments

We thank the NARL and IIG Allahabad airglow team members for carrying out night airglow imaging observations. The IGS-TEC hourly averaged data are downloaded from <https://cdaweb.sci.gsfc.nasa.gov/cgi-bin/eval2.cgi>. Excel files (.xlsx format) containing final derived airglow image data needed to reproduce the figures in this paper are provided in the supporting information. This work is supported by the Department of Space, Government of India.

- Cosgrove, R. B., Tsunoda, R. T., Fukao, S., & Yamamoto, M. (2004). Coupling of the Perkins instability and the sporadic E layer instability derived from physical arguments. *Journal of Geophysical Research*, *109*, A06301. <https://doi.org/10.1029/2003JA010295>
- Duly, T. M., Chapagain, N. P., & Makela, J. J. (2013). Climatology of nighttime medium-scale traveling ionospheric disturbances (MSTIDs) in the Central Pacific and South American sectors. *Annales Geophysicae*, *31*(12), 2229–2237. <https://doi.org/10.5194/angeo-31-2229-2013>
- Francis, S. H. (1974). A theory of medium-scale traveling ionospheric disturbances. *Journal of Geophysical Research*, *79*, 5245–5260. <https://doi.org/10.1029/JA079i034p05245>
- Fukushima, D., Shiokawa, K., Otsuka, Y., & Ogawa, T. (2012). Observation of equatorial nighttime medium-scale traveling ionospheric disturbances in 630-nm airglow images over 7 years. *Journal of Geophysical Research*, *117*, A10324. <https://doi.org/10.1029/2012JA017758>
- García, F. J., Kelley, M. C., Makela, J. J., & Huang, C.-S. (2000). Airglow observations of mesoscale low-velocity traveling ionospheric disturbances at midlatitudes. *Journal of Geophysical Research*, *105*, 18,407–18,415. <https://doi.org/10.1029/1999JA000305>
- Grocott, A., Hosokawa, K., Ishida, T., Lester, M., Milan, S. E., Freeman, M. P., et al. (2013). Characteristics of medium-scale traveling ionospheric disturbances observed near the Antarctic Peninsula by HF radar. *Journal of Geophysical Research: Space Physics*, *118*, 5830–5841. <https://doi.org/10.1002/jgra.50515>
- He, L., Dyson, P. L., Parkinson, M. L., Wan, W., & Wan, W. (2004). Studies of medium scale travelling ionospheric disturbances using TIGER SuperDARN radar sea echo observations. *Annales Geophysicae*, *22*(12), 4077–4088. <https://doi.org/10.5194/angeo-22-4077-2004>
- Hernández-Pajares, M., Juan, J. M., & Sanz, J. (2006). Medium-scale traveling ionospheric disturbances affecting GPS measurements: Spatial and temporal analysis. *Journal of Geophysical Research*, *111*, A07S11. <https://doi.org/10.1029/2005JA011474>
- Hines, C. O. (1960). Internal atmospheric gravity waves ionospheric heights. *Canadian Journal of Physics*, *38*(11), 1441–1481. <https://doi.org/10.1139/p60-150>
- Hocke, K., & Schlegel, K. (1996). A review of atmospheric gravity waves and travelling ionospheric disturbances: 1982–1995. *Annales Geophysicae*, *14*(9), 917–940. <https://doi.org/10.1007/s00585-996-0917-6>
- Hunsucker, R. D. (1982). Atmospheric gravity waves generated in the high-latitude ionosphere: A review. *Reviews of Geophysics*, *20*, 293–315. <https://doi.org/10.1029/RG020i002p00293>
- Jonah, O. F., Kherani, E. A., & De Paula, E. R. (2017). Investigations of conjugate MSTIDs over the Brazilian sector during daytime. *Journal of Geophysical Research: Space Physics*, *122*, 9576–9587. <https://doi.org/10.1002/2017JA024365>
- Kelley, M. C. (2011). On the origin of mesoscale TIDs at midlatitudes. *Annales Geophysicae*, *29*(2), 361–366. <https://doi.org/10.5194/angeo-29-361-2011>
- Kelley, M. C., & Makela, J. J. (2001). Resolution of the discrepancy between experiment and theory of midlatitude *F*-region structures. *Geophysical Research Letters*, *28*, 2589–2592. <https://doi.org/10.1029/2000GL012777>
- Kelley, M. C., Makela, J. J., Saito, A., Aponte, N., Sulzer, M., & González, S. A. (2000). On the electrical structure of airglow depletion/height layer bands over Arecibo. *Geophysical Research Letters*, *27*, 2837–2840. <https://doi.org/10.1029/2000GL000024>
- Kotake, N., Otsuka, Y., Ogawa, T., Tsugawa, T., & Saito, A. (2007). Statistical study of medium-scale traveling ionospheric disturbances observed with the GPS networks in Southern California. *Earth, Planets and Space*, *59*(2), 95–102. https://doi.org/10.1007/978-94-007-0326-1_21
- Kotake, N., Otsuka, Y., Tsugawa, T., Ogawa, T., & Saito, A. (2006). Climatological study of GPS total electron content variations caused by medium-scale traveling ionospheric disturbances. *Journal of Geophysical Research*, *111*, A04306. <https://doi.org/10.1029/2005JA011418>
- Krall, J., Huba, J. D., Ossakow, S. L., Joyce, G., Makela, J. J., Miller, E. S., & Kelley, M. C. (2011). Modeling of equatorial plasma bubbles triggered by non-equatorial traveling ionospheric disturbances. *Geophysical Research Letters*, *38*, L08103. <https://doi.org/10.1029/2011GL046890>
- Kubota, M., Conde, M., Ishii, M., Murayama, Y., & Jin, H. (2011). Characteristics of nighttime medium-scale traveling ionospheric disturbances observed over Alaska. *Journal of Geophysical Research*, *116*, A05307. <https://doi.org/10.1029/2010JA016212>
- MacDougall, J., Abdu, M. A., Batista, I., Fagundes, P. R., Sahai, Y., & Jayachandran, P. T. (2009). On the production of traveling ionospheric disturbances by atmospheric gravity waves. *Journal of Atmospheric and Solar-Terrestrial Physics*, *71*(17–18), 2013–2016. <https://doi.org/10.1016/j.jastp.2009.09.006>
- Makela, J. J., Miller, E. S., & Talaat, E. R. (2010). Nighttime medium-scale traveling ionospheric disturbances at low geomagnetic latitudes. *Geophysical Research Letters*, *37*, L24104. <https://doi.org/10.1029/2010GL045922>
- Makela, J. J., & Otsuka, Y. (2012). Overview of nighttime ionospheric instabilities at low- and mid-latitudes: Coupling aspects resulting in structuring at the mesoscale. *Space Science Reviews*, *168*(1–4), 419–440. <https://doi.org/10.1007/s11214-011-9816-6>
- Martinis, C., Baumgardner, J., Wroten, J., & Mendillo, M. (2010). Seasonal dependence of MSTIDs obtained from 630.0 nm airglow imaging at Arecibo. *Geophysical Research Letters*, *37*, L11103. <https://doi.org/10.1029/2010GL043569>
- Martinis, C., Baumgardner, J., Wroten, J., & Mendillo, M. (2011). All-sky imaging observations of conjugate medium-scale traveling ionospheric disturbances in the American sector. *Journal of Geophysical Research*, *116*, A05326. <https://doi.org/10.1029/2010JA016264>
- Maruyama, T., & Matuura, N. (1984). Longitudinal variability of annual changes in activity of equatorial spread *F* and plasma bubbles. *Journal of Geophysical Research*, *89*, 10,903–10,912. <https://doi.org/10.1029/JA089iA12p10903>
- Miller, C. A., Swartz, W. E., Kelley, M. C., Mendillo, M., Nottingham, D., Scali, J., & Reinisch, B. (1997). Electrodynamic of midlatitude spread *F*, 1. Observations of unstable, gravity wave-induced ionospheric electric fields at tropical latitudes. *Journal of Geophysical Research*, *102*, 11,521–11,532. <https://doi.org/10.1029/96JA03839>
- Moffett, R. J., & Balthazor, R. L. (1997). A study of atmospheric gravity waves and travelling ionospheric disturbances at equatorial latitudes. *Annales Geophysicae*, *15*(8), 1048–1056. <https://doi.org/10.1007/s00585-997-1048-4>
- Mukherjee, G. K., Parihar, N., Niranjana, K., & Manju, G. (2006). Signature of midnight temperature maximum (MTM) using OI 630 nm airglow. *Indian Journal of Radio & Space Physics*, *35*(1), 14–21.
- Narayanan, V., Shiokawa, K., Otsuka, Y., & Saito, S. (2014). Airglow observations of nighttime medium-scale traveling ionospheric disturbances from Yonaguni: Statistical characteristics and low-latitude limit. *Journal of Geophysical Research: Space Physics*, *119*, 9268–9282. <https://doi.org/10.1002/2014JA020368>
- Negrea, C., Zabolin, N., & Bullett, T. (2018). Seasonal variability of the midlatitude traveling ionospheric disturbances from Wallops Island, VA, Dynasonde data: Evidence of a semiannual variation. *Journal of Geophysical Research: Space Physics*, *123*, 5047–5054. <https://doi.org/10.1029/2017JA025164>
- Otsuka, Y., Onoma, F., Shiokawa, K., Ogawa, T., Yamamoto, M., & Fukao, S. (2007). Simultaneous observations of nighttime medium-scale traveling ionospheric disturbances and *E* region field-aligned irregularities at midlatitude. *Journal of Geophysical Research*, *112*, A06317. <https://doi.org/10.1029/2005JA011548>

- Otsuka, Y., Shiokawa, K., & Ogawa, T. (2012). Disappearance of equatorial plasma bubble after interaction with mid-latitude medium-scale traveling ionospheric disturbance. *Geophysical Research Letters*, *39*, L14105. <https://doi.org/10.1029/2012GL052286>
- Otsuka, Y., Shiokawa, K., Ogawa, T., & Wilkinson, P. (2004). Geomagnetic conjugate observations of medium-scale traveling ionospheric disturbances at midlatitude using all-sky airglow imagers. *Geophysical Research Letters*, *31*, L15803. <https://doi.org/10.1029/2004GL020262>
- Otsuka, Y., Suzuki, K., Nakagawa, S., Nishioka, M., Shiokawa, K., & Tsugawa, T. (2013). GPS observations of medium-scale traveling ionospheric disturbances over Europe. *Annales Geophysicae*, *31*(2), 163–172. <https://doi.org/10.5194/angeo-31-163-2013>
- Parihar, N., Maria Radicella, S., Nava, B., Olivia Migoya-Orue, Y., Tiwari, P., & Singh, R. (2018). An investigation of the ionospheric F region near the EIA crest in India using OI 777.4 and 630.0 nm nightglow observations. *Annales Geophysicae*, *36*(3), 809–823. <https://doi.org/10.5194/angeo-36-809-2018>
- Paulino, I., Medeiros, A. F., Vadas, S. L., Wrasse, C. M., Takahashi, H., Buriti, R. A., et al. (2016). Periodic waves in the lower thermosphere observed by OI 630 nm airglow images. *Annales Geophysicae*, *34*(2), 293–301. <https://doi.org/10.5194/angeo-34-293-2016>
- Perkins, F. (1973). Spread F and ionospheric currents. *Journal of Geophysical Research*, *78*, 218–226. <https://doi.org/10.1029/JA078i001p00218>
- Röttger, J. (1977). Travelling disturbances in the equatorial ionosphere and their association with penetrative cumulus convection. *Journal of Atmospheric and Terrestrial Physics*, *39*(9–10), 987–998. [https://doi.org/10.1016/0021-9169\(77\)90007-1](https://doi.org/10.1016/0021-9169(77)90007-1)
- Saito, A., Iyemori, T., Sugiura, M., Maynard, N. C., Aggson, T. L., Brace, L. H., et al. (1995). Conjugate occurrence of the electric-field fluctuations in the nighttime midlatitude ionosphere. *Journal of Geophysical Research*, *100*, 21,439–21,451. <https://doi.org/10.1029/95JA01505>
- Saito, S., Yamamoto, M., Hashiguchi, H., Maegawa, A., & Saito, A. (2007). Observational evidence of coupling between quasi-periodic echoes and medium scale traveling ionospheric disturbances. *Annales Geophysicae*, *25*(10), 2185–2194. <https://doi.org/10.5194/angeo-25-2185-2007>
- Sau, S., Narayanan, V. L., Gurubaran, S., & Emperumal, K. (2018). Study of wave signatures observed in thermospheric airglow imaging over the dip equatorial region. *Advances in Space Research*, *62*(7), 1762–1774. <https://doi.org/10.1016/j.asr.2018.06.039>
- Shiokawa, K., Ihara, C., Otsuka, Y., & Ogawa, T. (2003). Statistical study of nighttime medium-scale traveling ionospheric disturbances using midlatitude airglow images. *Journal of Geophysical Research*, *108*(A1), 1052. <https://doi.org/10.1029/2002JA009491>
- Shiokawa, K., Otsuka, Y., Ejiri, M. K., Sahai, Y., Kadota, T., Ihara, C., et al. (2002). Imaging observations of the equatorward limit of midlatitude traveling ionospheric disturbances. *Earth, Planets and Space*, *54*(1), 57–62. <https://doi.org/10.1186/BF03352421>
- Shiokawa, K., Otsuka, Y., Ihara, C., Ogawa, T., & Rich, F. J. (2003). Ground and satellite observations of nighttime medium-scale traveling ionospheric disturbance at midlatitude. *Journal of Geophysical Research*, *108*(A4), 1145. <https://doi.org/10.1029/2002JA009639>
- Shiokawa, K., Otsuka, Y., & Ogawa, T. (2006). Quasiperiodic southward moving waves in 630-nm airglow images in the equatorial thermosphere. *Journal of Geophysical Research*, *111*, A06301. <https://doi.org/10.1029/2005JA011406>
- Shiokawa, K., Otsuka, Y., Tsugawa, T., Ogawa, T., Saito, A., Ohshima, K., et al. (2005). Geomagnetic conjugate observation of nighttime medium- and large-scale traveling ionospheric disturbances: FRONT3 campaign. *Journal of Geophysical Research*, *110*, A05303. <https://doi.org/10.1029/2004JA010845>
- Taori, A., Jayaraman, A., & Kamalakar, V. (2013). Imaging of mesosphere-thermosphere airglow emissions over Gadanki (13.5°N, 79.2°E) — First results. *Journal of Atmospheric and Solar-Terrestrial Physics*, *93*, 21–28. <https://doi.org/10.1016/j.jastp.2012.11.007>
- Taori, A., Parihar, N., Ghodpage, R., Dashora, N., Sripathi, S., Kherani, E. A., & Patil, P. T. (2015). Probing the possible trigger mechanisms of an equatorial plasma bubble event based on multistation optical data. *Journal of Geophysical Research: Space Physics*, *120*, 8835–8847. <https://doi.org/10.1002/2015JA021541>
- Tsugawa, T., Otsuka, Y., Coster, A. J., & Saito, A. (2007). Medium-scale traveling ionospheric disturbances detected with dense and wide TEC maps over North America. *Geophysical Research Letters*, *34*, L22101. <https://doi.org/10.1029/2007GL031663>
- Tsunoda, R. T., & Cosgrove, R. B. (2001). Coupled electrodynamics in the nighttime midlatitude ionosphere. *Geophysical Research Letters*, *28*, 4171–4174. <https://doi.org/10.1029/2001GL013245>
- Valladares, C. E., & Sheehan, R. (2016). Observations of conjugate MSTIDs using networks of GPS receivers in the American sector. *Radio Science*, *51*, 1470–1488. <https://doi.org/10.1002/2016RS005967>